Notch-Defect Interaction in Additively Manufactured Inconel 718

K. Solberg, F. Berto

PII: S0142-1123(18)30738-2
DOI: https://doi.org/10.1016/j.ijfatigue.2018.12.021
Reference: JIJF 4935

To appear in: *International Journal of Fatigue*

Revised Date: 20 December 2018
Accepted Date: 22 December 2018

Please cite this article as: Solberg, K., Berto, F., Notch-Defect Interaction in Additively Manufactured Inconel 718, *International Journal of Fatigue* (2018), doi: https://doi.org/10.1016/j.ijfatigue.2018.12.021

Notch-Defect Interaction in Additively Manufactured Inconel 718

K. Solberg[a,*], F. Berto[a]

[a]*Department of Mechanical and Industrial Engineering, Norwegian University of Science and Technology, 7034 Trondheim, Norway*

Abstract

Powder bed fusion based additively manufactured components are known to have poor surface quality, especially when building downward facing surfaces. These surfaces can contain defects, from which fatigue cracks can be initiated. In this work the notched fatigue behaviour of Inconel 718 specimens produced by selective laser melting is investigated. The main focus is set on the interaction between notch geometries and local defects due to the amount of overhang in the notch region. Four different geometries are considered, with different amount of notch acuities and degree of downward facing surfaces. A variation in failure sites, with respect to the notch bisector line, was fond in the specimens, and the position was found to be dependent on the amount of overhang and notch acuity. The fatigue life was found to be dependent on the size of surface defects measured in fracture surfaces. Further, the use of average strain energy density as a failure criteria in additively manufactured metals is discussed.

Keywords: Fatigue, Additive Manufacturing, Fracture, Defect, Surface

1. Introduction

Additive Manufacturing (AM) is a manufacturing method, producing components by adding material in a layer-by-layer manner. Components of high complexity can be produced, based on computer-aided designs. However, for Powder Bed Fusion (PBF) based AM methods, components are displaying poor surface quality, especially when building downward facing surfaces [1–7]. With increasing interest in using AM components in engineering applications, it is necessary to evaluate the structural integrity of the respective components [8]. A schematic illustration of manufacturing process and as-built part is shown in Fig. 1.

The structural integrity for a wide range of AM metals has previously been studied [2, 3], the general trend is that as-built specimens are showing the lowest strength and mechanical properties. Different post-processing methods can increase the mechanical properties [4]. Typical post-processing employed to increase the mechanical properties are heat treatment, Hot Isostatic Pressing (HIPing), and machining [2, 9]. Heat treatment can remove residual

*Corresponding author
Email address: klas.solberg@ntnu.no (K. Solberg)

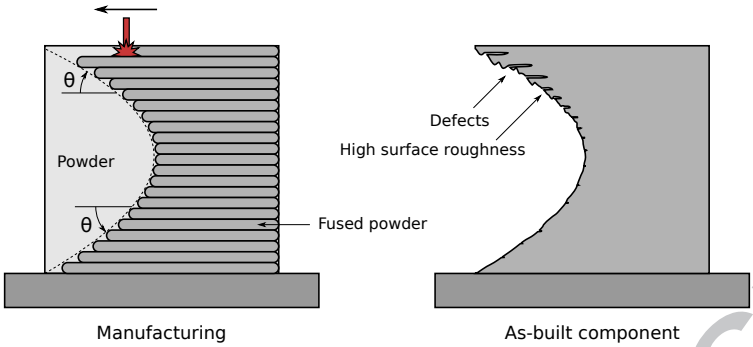

Figure 1: Schematic illustration of Manufacturing and as-built additive manufactured component. The as-built component has defects and poor surface quality in regions built with downward facing surfaces.

stresses and alter the microstructure. HIPing can close internal voids, such as lack of fusion and gas pores; however, defects open to the surface will not be closed [10]. Machining the surface will remove the outer layer of the material, generally found to have high surface roughness and defects [2, 3, 11]. In the case of fatigue, especially for high strength metals, geometrical defects and surface roughness is a major factor determining the fatigue life [4, 12, 13]. Relating geometrical defects to the fatigue behaviour, several papers [13–17] are recently employing the $\sqrt{\text{area}}$-method developed by Murakami [18]. The method is based on measuring the effective size of the defect found in the fracture surface, then relating this effective size to the fatigue life of the component.

With the new allowed degree of complexity in components by use of AM, engineers are looking into combining components, topology optimisation and grid structures [8]. This increase in geometrical complexity makes it more challenging to evaluate stresses in a Finite Element (FE) model, as refine meshes are needed. Because of this, failure criteria independent of the mesh are desirable. Average Strain Energy Density (ASED) is a failure assessment method used for brittle fracture in static and cyclic loading for the assesment of fracture and fatigue failures, evaluating the average value of Strain Energy Density (SED) within a fixed control volume surrounding the notch tip [19]. When applied in FE models it has low sensitivity to the mesh size [19–22]. The possibility of employing ASED for AM metals has previously been investigated by Razavi et al. [23]. ASED has previously been employed on welded joints, which similar to AM metals contain residual stresses and defects [19].

Inconel 718 is a Ni-based superalloy, with high strength and fatigue properties at a wide range of temperatures [24, 25]. The material is commonly used for turbine blades, pipeline components, aerospace components and other applications requiring high mechanical properties at extreme temperatures. Inconel 718 is a high strength material and with AM it can be manufactured to near-net shaped components, reducing the need of machining. Reported results of AM Inconel 718 shows poor resistance to crack growth in the threshold region and fatigue cracks are initiating from defects such as lack of fusion [4, 17, 26, 27].

In this work notched fatigue behaviour of as-built Inconel 718 specimens produced by SLM is investigated. Four different specimen geometries with different notch radii and

amounts of overhang is considered. The paper is aiming to (1) Describe the relationship between fatigue life and surface defects for notched and unnotched specimens. (2) Propose a model relating the position of crack initiation site, in terms of height with respect to the notch bisector line, to the degree of overhang in a notch geometry. (3) Investigating the challenges and opportunities of applying ASED as a failure criterion in AM components.

2. Theoretical background

The first proposal of local approach for evaluating failure was Neuber's concept of elementary structural volume and microstructural support length [28, 29]. The main idea is from these concepts is that static or fatigue failure is governed not by the theoretical maximum stress in the notch, but rather the stress in the vicinity of the notch averaged over a volume or a length close to the notch root. The first proposal of strain energy as a failure criterion was by Beltrami in 1885 [30], stating that failure occurs when the level of strain energy reaches a critical value. Further, Sih proposed, for cracks, to evaluate a parameter dependent on SED and a critical distance from the crack tip singularity [31]. Where crack propagation would occur if the value of SED were equal to the critical value for the material. The theory was further extended to notches, using a reference point at the notch surface, where the tangential stress component has the maximum value. The SED failure criterion was refined and formulated in [32].

ASED proposed by Lazzarin and Zambardi [33] evaluates SED in a defined control volume surrounding the notch tip. The criterion states that failure occurs when the mean value of SED, $\bar{W}$, over the control volume is equal to the critical value of energy for the material, W_c:

$$\bar{W} = W_c. \tag{1}$$

Based on the coordinate system of Lazzarin and Tovo [34], the control volume is defined for cracks, sharp notches and blunt notches. The generalised definition of the control volume is shown in Fig. 2, for sharp and blunt notches. ρ is the notch root radius, 2α is the opening angle of the notch, R_0 is the critical radius defining the size of the control volume, this parameter is dependent on the material and r_0 defines the centroid of control volume.

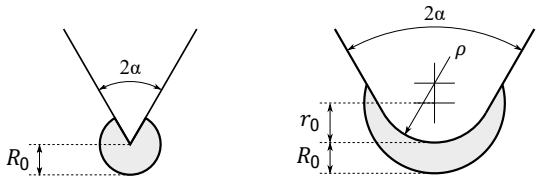

Figure 2: Generalized notch geometry and control volume used for average strain energy density.

In the case of static loading for a plain specimen, failure is evaluated by use of the ultimate tensile strength, σ_t, and Young's modulus, E, of the material.

$$W_c = \frac{\sigma_t^2}{2E}. \tag{2}$$

In the case of sharp notches, ASED can be evaluated analytically for mode I loading by referring to the generalised notch stress intensity factor, K_I^V

$$\bar{W}_I = \frac{I_1}{4E\lambda_1(\pi-\alpha)}\left(\frac{K_I^V}{R_0^{1-\lambda_I}}\right)^2, \tag{3}$$

where I_1 is a parameter dependent on the opening angle of the notch and λ_1 is the Williams' series eigenvalue [35]. In the case of blunt notches, ASED can be calculated analytically for mode I loading by referring to the maximum stress at the notch tip σ_{max}

$$\bar{W}_I = F(2\alpha) \times H\left(2\alpha, \frac{R_0}{\rho}\right) \times \frac{\sigma_{max}^2}{E}, \tag{4}$$

where F is a function dependent on 2α and H is a function dependent on 2α and the ratio between R_0/ρ [19]. ASED has previously been employed on a wide range of materials and loading conditions, including multi-axial fatigue of Ti6Al4V [19, 36–38].

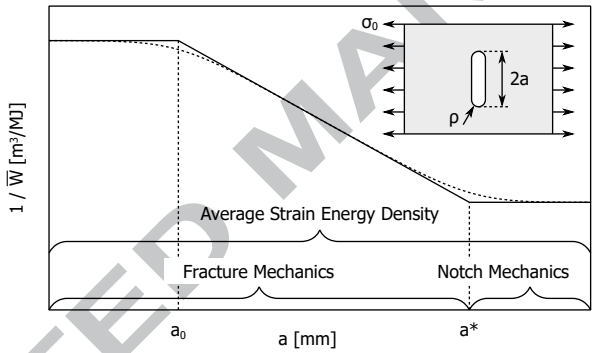

Figure 3: Schematic illustration of Atzori-Lazzarin diagram [39, 40], inverse of average strain energy density versus defect size.

The Atzori-Lazzarin diagram [39, 40], an extension of Kitagawa-Takahashi diagram [41] has interesting applications for AM materials. The diagram is evaluating ASED at the fatigue limit for different notch/crack sizes, a. A schematic illustration of the diagram is shown in Fig. 3. The diagram consists of two plateaus of $1/\bar{W}$ and a transition between them. The diagram can easily be understood by considering an arbitrary defect in a material, with constant notch acuity a/ρ, where a is the size (depth) of the defect and ρ is the notch radius of the defect. For a defect with size less than a_0, the defect will not influence the fatigue limit. For a defect size larger than a^*, the defect is acting as a notch, and linear notch mechanics can be applied. In the transition region between these two plateaus, the defect is affecting fatigue behaviour and should be taken into account locally, by applying linear elastic fracture mechanics.

AM components and specimens can contain global defects, such as notches, and at the same time local defects, such as lack of fusion or pores. Looking to models such as the Atzori-Lazzarin diagram, taking into account the whole range of defects in the fatigue assessment, combining notch mechanics and fracture mechanics can be useful in future applications when developing tools determining the fatigue life of AM components.

3. Experimental procedure, testing and material

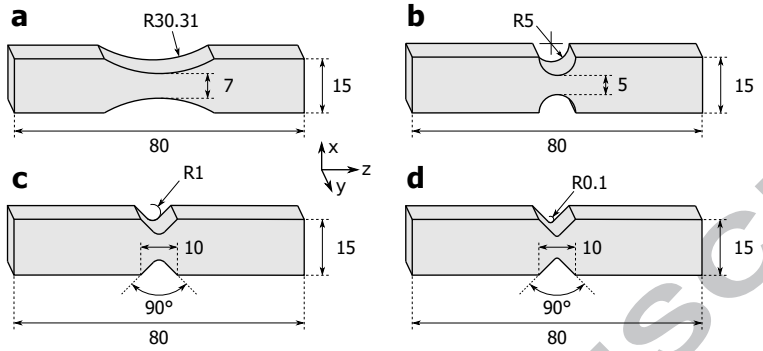

Figure 4: Specimen geometries: (a) Unnotched; (b) semi-circular notch; (c) v-shaped notch with notch radius equal to 1 mm; (d) v-shaped notch with notch radius equal to radius 0.1 mm. Notch depth of specimens: 4 mm, 5 mm, 4.59 mm and 4.96 mm for (a), (b), (c) and (d) respectively.

The fatigue behaviour of four different specimen geometries of AM Inconel 718 produced by SLM was investigated. The geometry of the different specimens is shown in Fig. 4. An unnotched specimen geometry was compared to three double notch specimen geometries; semi-circular, v-shaped notch with a radius equal to 1 mm and v-shaped notch with a radius equal to 0.1 mm. All specimens were of 5 mm thickness. The specimen geometries investigated was based on notch geometries proposed by Pilkey et al. [42]. The specimens were produced by SLM, by use of standardised processing parameters on an SLM Solution system. The specimens were build to a solid layer by layer in the z-direction, referring to coordinate system in Fig. 4, with a layer height of 50 μm and energy density of 60 J/mm^3. No distortion was found in the specimens potentially causing misalignments in the fatigue testing, like what has been reported previously in literature for additively manufactured cylindrical maraging steel specimens of comparable dimensions [15].

Specimens were tested for high cycle fatigue under uniaxial loading on an MTS Landmark Servohydraulic test system, with a loading ratio $R = 0$ and a frequency of 10 Hz. The tests were performed at room temperature. Specimens that did not fail after 2×10^6 cycles were considered as run out, and the fatigue strength was evaluated at this number of cycles. The fatigue data obtained was presented in S-N diagrams, with scatter bands at 2.3 %, 50 % and 97.7% probability of failure.

The surface roughness of surfaces build in different orientations was measured in terms of R_a on an Alicona Infinite Focus Microscope. Surface roughness was evaluated for v-notch specimens, on surfaces built vertical, upward facing (45°) and downward facing (45°). The surface roughness was evaluated along lines of 4 mm. The microstructure of the material was obtained by polishing and etching according to ASTM E407-07, with etchant 94 [43]. Fractography was performed by the means of SEM. Fracture surfaces were analysed, and the area of the defects found to initiate fatigue was measured. In the cases that the edge of the specimens were hard to define, regions displaying clear signs of lack of fusion close to or in contact with the surface, were measured. The position of failure in the notch region,

with respect to the notch bisector line, was measured for all specimens. As uniaxial loading was applied, the fracture surfaces were flat for the crack growth region, according to mode I loading.

The elastic stress concentration factor, K_t, was determined for the different geometries by use of the Finite Element (FE) software Abaqus. Two-dimensional models were made, assuming plane strain conditions and utilising symmetry in the specimens. The stress concentration factor was obtained by evaluating ratio of the maximum stress at the notch root and the nominal stress in the net cross-sectional area of the notch. The material was considered to obey a linear elastic behaviour, with Young's modulus and the Poisson ratio equal to 200 GPa and 0.29, respectively [44]. The fatigue reduction factor, K_f, was obtained for the different geometries by evaluating $K_f = \Delta\sigma^S/\Delta\sigma^N$, where $\Delta\sigma^S$ and $\Delta\sigma^N$ is the unnotched and notched fatigue strength at 2×10^6 cycles, respectively. The notch sensitivity, q, was evaluated by $q = (K_f - 1)/(K_t - 1)$.

ASED of the different geometries was done using the same FE model as used for evaluating the stresses. The volume for evaluating the ASED was created according to Fig. 2. In order to give an estimation of the control volume for the material, ASED of the unnotched specimen was evaluated at the fatigue limit by means of Eq. (2). Referring to this value, the control volume giving the corresponding value of ASED for v-notch specimens with 0.1 mm radius was determined.A similar approach for determining critical distance in critical distance theory and critical radius ASED previously reported in literature [45, 46]. ASED-analysis was performed for a unit load, and then the result obtained for each geometry was scaled to the correct load level, for each fatigue data, by means of Eq. (2).

4. Results

4.1. Fatigue data

	$\Delta\sigma$ - 97.7%	$\Delta\sigma$ - 50%	$\Delta\sigma$ - 2.3%	K_t	K_f	q
Unnotched	168.93	250.00	369.99	1.07	-	-
Semicircular	151.88	175.40	202.58	1.31	1.42	1.35
V-notch ρ=1	105.77	121.33	139.17	2.43	2.06	0.74
V-notch ρ=0.1	92.76	100.44	108.74	6.28	2.49	0.24

Table 1: Values for confidence bands at 2×10^6 cycles, elastic stress concentration factor, K_t (referring to net cross sectional area), fatigue notch factor, K_f, and fatigue notch sensitivity, q.

The fatigue data for all specimen geometries are presented by means of S-N diagrams in Fig. 5, with confidence bands at 2.3 %, 50 % and 97.7 % probability of failure. The fatigue strength of unnotched specimens was 250 MPa, the fatigue strength was then reduced with decreasing notch radius; 175 MPa for the semi-circular notch, 121 MPa for v-notch with 1 mm radius and 100 MPa for v-notch with 0.1 mm radius. The inverse slope of the confidence bands, k, and scatter parameter, $T_{\Delta\sigma}$, are shown in the plots. The scatter parameter is decreasing as the notch radius decreases. The inverse slope of the confidence bands is 3.67,

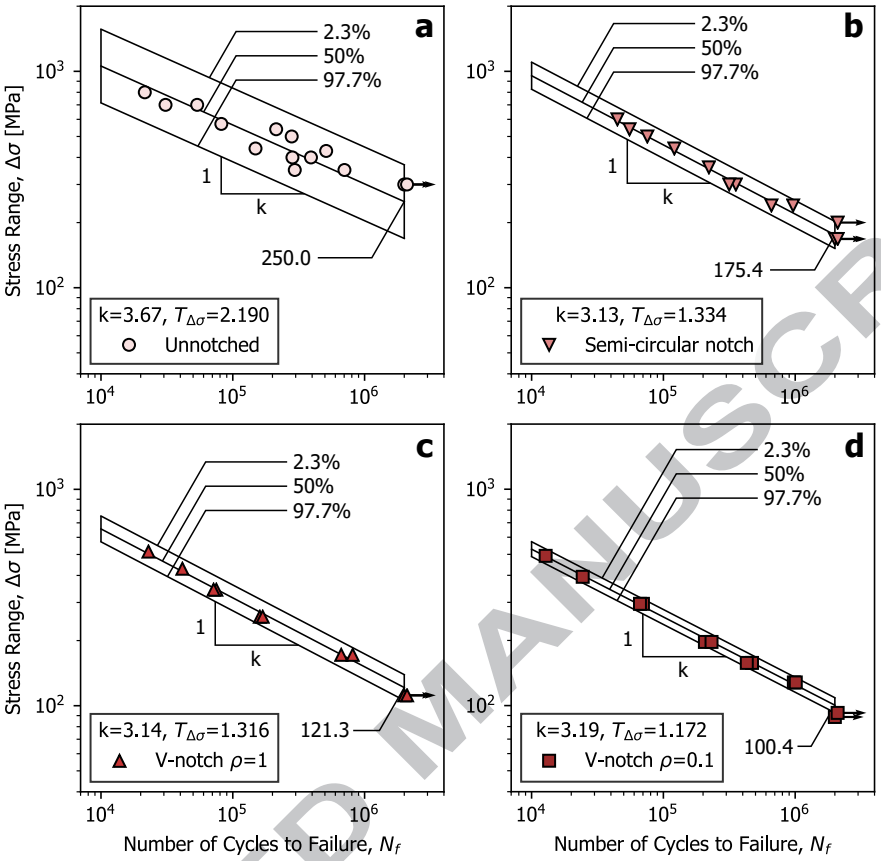

Figure 5: Fatigue data obtained for different specimen geometries tested with loading ratio R=0: (a) Unnotched; (b) Semi-circular notch; (c) v-notch 1 mm radius; (d) v-notch 0.1 mm radius.

3.13, 3.14 and 3.19 for unnotched, semi-circular, v-shaped notch with 1 mm radius and v-shaped notch with 0.1 mm radius, respectively. The slope is similar for the different notch geometries, while it is lower for the unnotched specimens. Fatigue strength at 2×10^6 cycles for the different confidence bands are shown in Table 1, for all geometries.

4.2. Notch Sensitivity

The elastic stress concentration factor, the fatigue notch factor and the notch sensitivity are compared and shown in Table 1. The fatigue strength was reduced as the stress concentration factor was increased. V-notch with a radius of 0.1 mm showed the highest fatigue notch factor, then the v-shaped notch with 1 mm radius and then the semi-circular notch. For v-notch geometries the fatigue notch factor were smaller than the stress concentration factor, while for the semi-circular notch, the fatigue notch factor was higher than the stress concentration factor, i.e. a notch sensitivity above 1, taking the unnotched specimen as a reference.

4.3. Surface Roughness and Microstructure

The surface roughness of different regions was measured. For v-notch specimens, the vertical built surface and upward facing surface of the notch was measured to be 3.08 μm

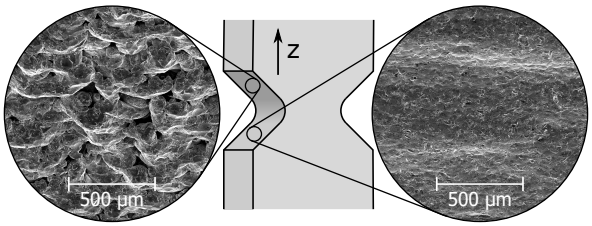

Figure 6: SEM of surface build facing downwards and upwards.

and 3.20 μm respectively. The downward facing surface of the notch was measured to have a surface roughness of 20.95 μm. Fig. 6 shows SEMs of upward and downward facing surfaces.

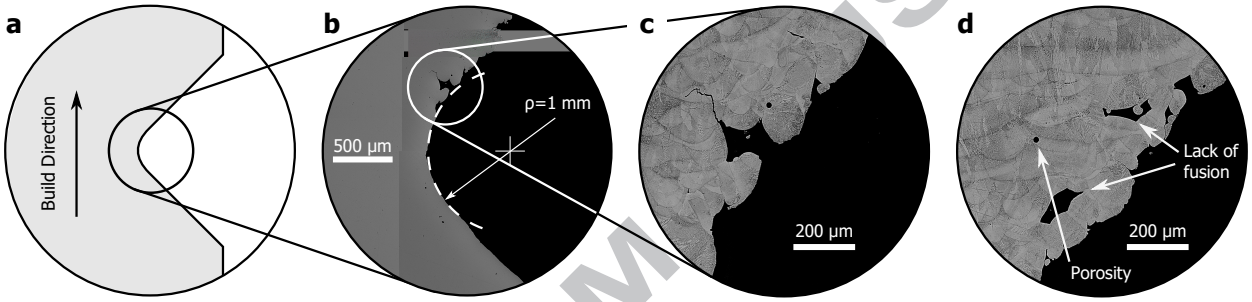

Figure 7: V-notch specimen with 1 mm radius tested until 2×10^6 cycles; (a) Schematic illustration of notch and build direction; (b) Optical micrograph of centre plane of specimen, polished; (c) Microstructure and defect initiating fatigue crack growth; (d) Microstructure and defects in downward facing region.

The notched region of a v-notch specimen loaded until 2×10^6 cycles is shown in Fig. 7. From Fig. 7b the geometry in the notch root is shown, in the overhanging region the surface is rougher, and defects are present. From one of the defects in the overhanging region a fatigue crack can be seen. This fatigue crack and the microstructure of the material is shown with a higher magnification in Fig. 7c. The defect from which the fatigue crack is growing is of depth $\sim$200 μm. Fig. 7d shows a porosity and lack of fusion defects in the downward facing surface. In Fig. 7c and d the microstructure of the material is shown, cross sections of the melt pools and elongated grains growing across the melt pools are visible.

4.4. Fractography

Fractography was conducted by means of SEM of all fracture surfaces. One fracture surface of each geometry is shown in Fig. 8a-d. Arrows indicates the crack growth and dashed lines indicates the transition from fatigue crack growth to final rupture. The general trends in the fracture surfaces are: (1) Unnotched specimens have crack initiation on one side of the specimen. In the fracture surfaces small defects were found, as seen in Fig. 8e. (2) Semi-circular notch specimens failed from one side, and lack of fusion defects were found at crack initiation site. (3) V-shaped notch specimens with notch radii of 1 and 0.1 mm failed from both sides of the specimen, and lack of fusion defects was found at crack initiation site, as seen in Fig. 8f.

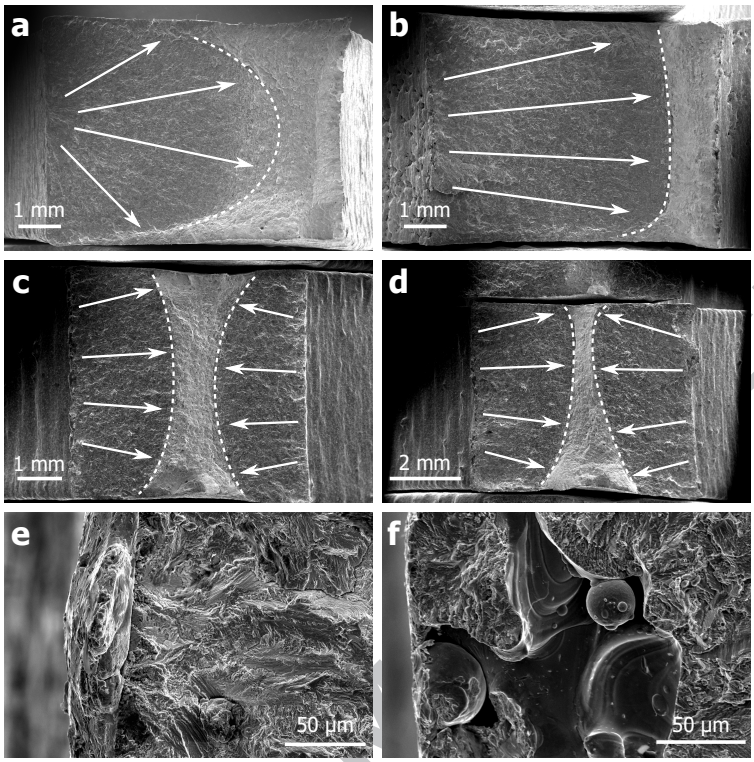

Figure 8: Fracture surface for different specimen: (a) Unnotched speicmen, crack growth from one side; (b) Semi-circular notch, crack growth from one side; (c) v-notch 1 mm radius, crack growth from both sides; (d) v-notch 0.1 mm radius, crack growth from both sides; (e) Defect from unnotched specimen; (f) Defect from v-notch specimen with 1 mm radius, lack of fusion defect, unfused powder particle visible.

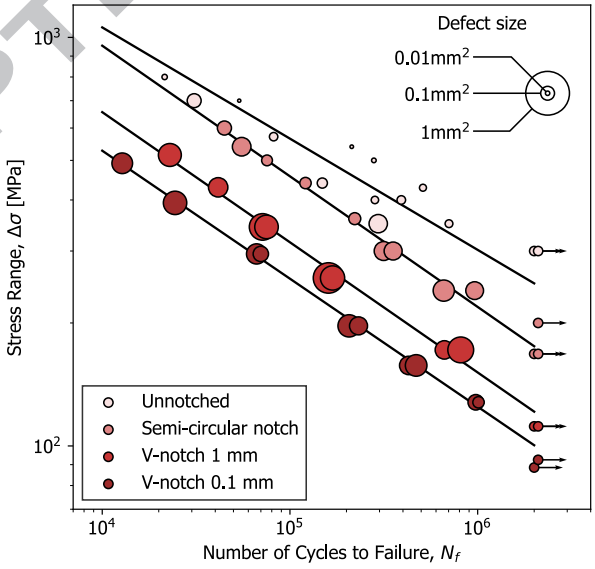

Figure 9: Fatigue data for all specimen geometries, with marker size as measured defect area from crack initiation. Loading ratio R=0.

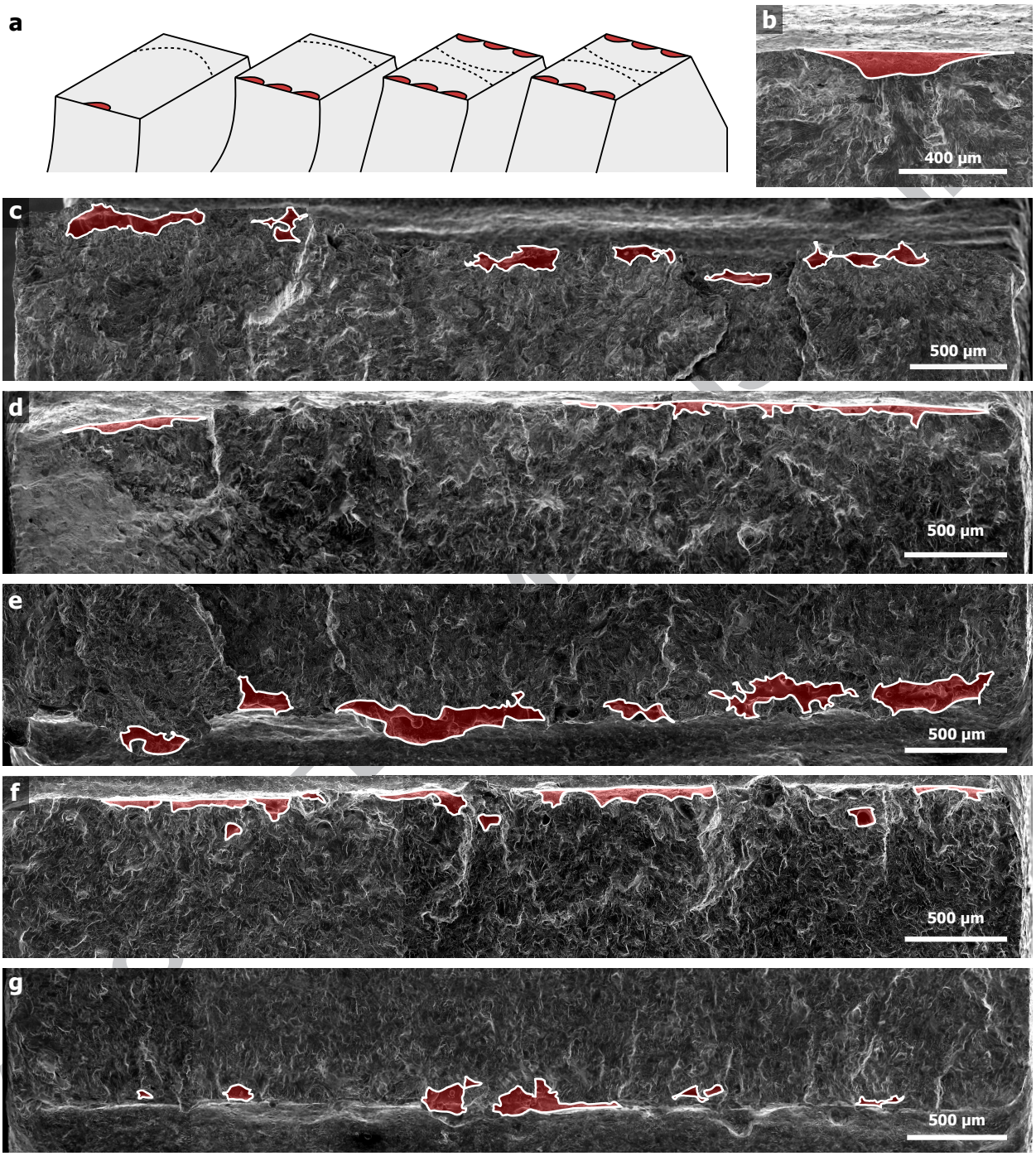

Figure 10: (a) Schematic illustration of fracture surface of unnotched, semi-circular, and v-notch specimens. Fractography of defects in specimens: (b) unnotched; (c) semi-circular; (d, e) v-notch radius 1 mm; (f, g) v-notch radius 0.1 mm.

All specimens were found to have crack initiation from surface defects, none of the specimens had crack inidistotiating from internal defects. The surface defects of all the

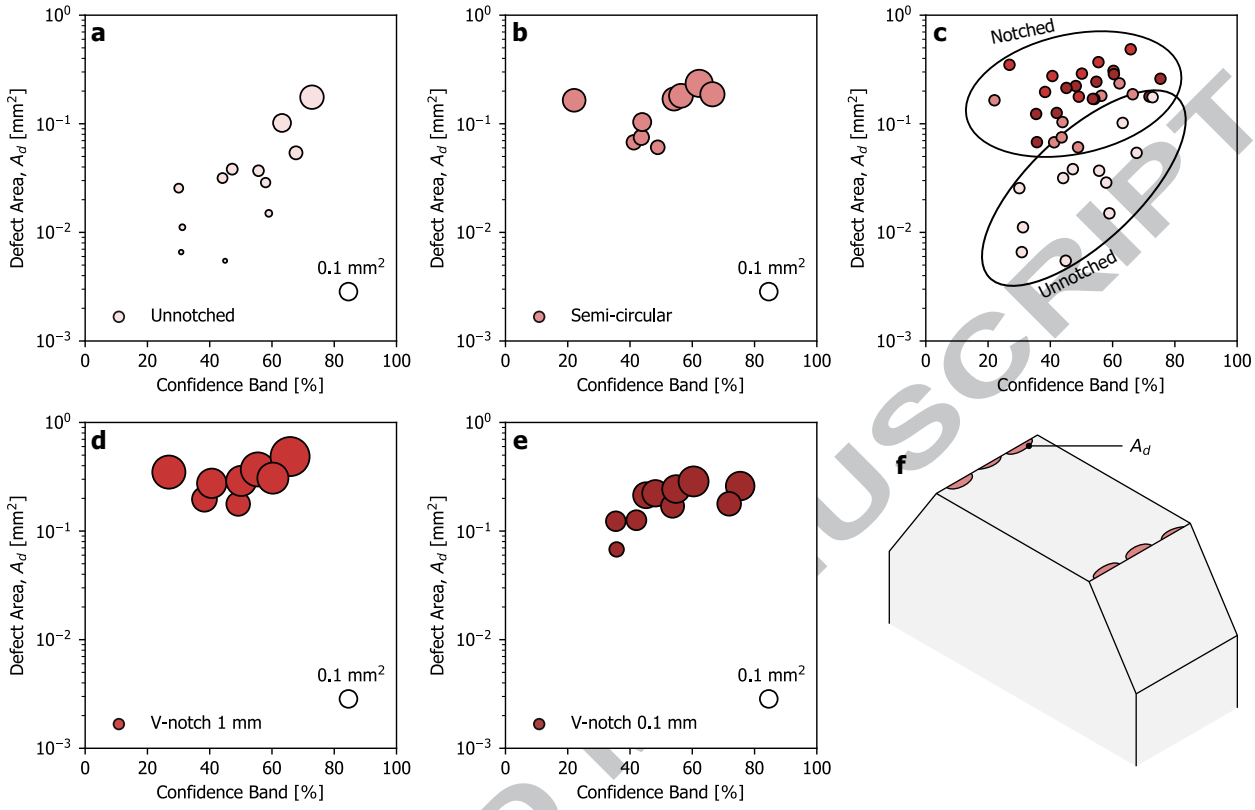

Figure 11: Dependency between defect size initiating fatigue and placement in scatter band: (a,b,d,e) Unnotched specimen, semi-circular specimen, v-notch 1 mm radius and v-notch 0.1 mm radius respectively; (c) All specimens; (f) Schematic illustration of cross section and defect size, A_d.

specimens were captured by SEM, and the area of each defect initiating crack growth was measured. The total area of defects in the surface region of each specimen was measured, giving a simple representation of the measurable defect size. Fig. 9 shows the fatigue data for all specimens, where the marker is plotted as the size of the surface defect. In Fig. 10, the measured defect area is shown for one specimen of each geometry, the defects are marked in red.

In order to further investigate the relation between the fatigue life and the defect size, the position of each fatigue data with respect to the confidence band was plotted versus the defect size, this is shown in Fig. 11a, b, d and e. Here the marker size is indicating the size of the defects, A_d, measured. A comparison of the defect size in the different specimens is shown in Fig. 11c.

4.5. Failure Site

Generally, for notched components, the crack initiation site is at the position of the maximum stress, i.e. the notch root for mode I loading. The specimens investigated here did not show this typical behaviour. The failure was often occurring from the downward facing surface region, and as seen in the previous section, the specimens failed from surface defects such as lack of fusion. The position of the failure site was measured in the build

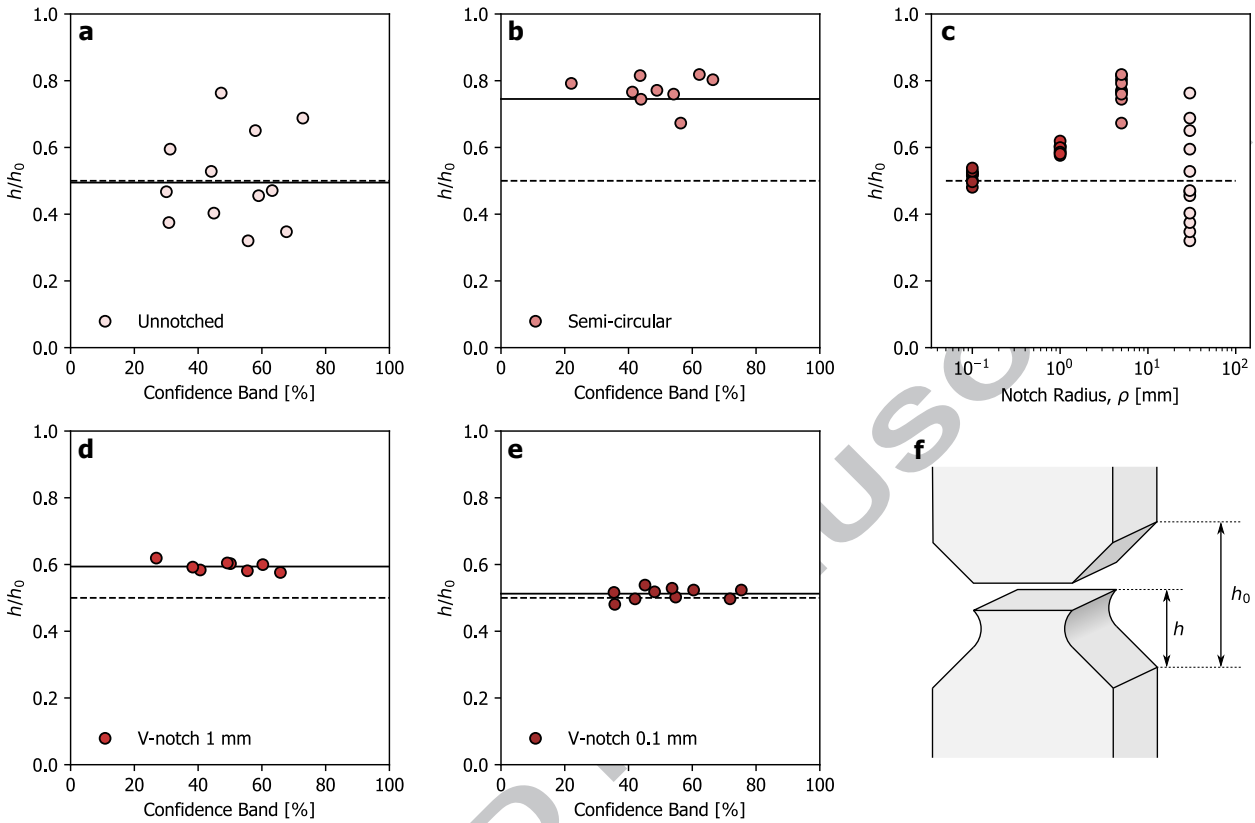

Figure 12: Failure initiation site for different specimens: (a,b,d,e) Height of failure for the different geometries; (c) Failure site versus notch radius; (f) Schematic illustration of relative height in notch.

direction for all specimens. The relative height in the notch was considered by h/h_0, where h is the height of failure initiation in build direction, and h_0 is the total height of the notch, as defined in Fig. 12f. The failure site, measured as relative height in the notch, was further compared with the position of the specimen in the confidence bands. The result is shown in Fig. 12a, b, d and e. In the plots, the dashed lines are indicating the notch bisector line.

In the unnotched specimens failure is occurring with a large scatter in h/h_0. The semi-circular specimens are failing from the overhang region, with less scatter than the unnotched. For the v-notches, the failure is approaching the notch root as the notch radius decreases. The failure site was plotted versus the radius of the notch in Fig. 12c. The following observations were made: (1) The general trend is that as the notch radius decreases, the scatter decreases. (2) There is no dependency between confidence bands and failure site, unlike what was seen when evaluating defect size. (3) With a blunt notch and high amount of overhang the specimens are failing from the overhang region.

4.6. Strain Energy Density

ASED analysis were performed in Abaqus. The results for ASED analysis are shown in Fig. 13a and b, with $R_0 = 0.13$ mm. In Fig. 13a, ASED are shown for the fatigue data of both v-notches, while in b, the fatigue data for semi-circular specimens are added.

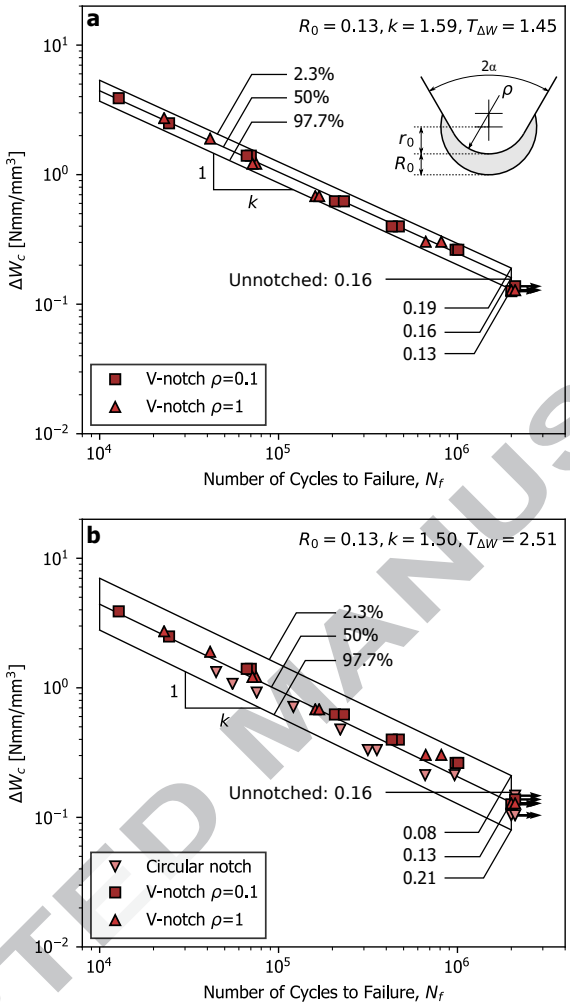

Figure 13: ASED versus number of cycles to failure for: (a) V-notch specimens;(b) All notch specimens

Confidence bands at 2.3 %, 50 % and 97.7 % are shown in the plots. ASED of the fatigue data are presented in a scatter bands with scatter parameter $T_{\Delta W} = 1.45$ and inverse slope $k = 1.45$ for the first case and $T_{\Delta W} = 2.51$ and $k = 1.50$ for the second case.

5. Discussion

Fatigue behaviour for different notch geometries of AM Inconel 718 has been studied. Fractography was conducted by SEM, and all specimens were found to fail from defects in the surface region. Failure initiation site, as relative height in the notch, was obtained for all specimens. For decreasing notch radius, decreasing scatter in failure initiation site was obtained. Based on the defects found in fracture surfaces, and the failure initiation sites, it is believed that there are two main competing factors for crack initiation in the specimens; local and global notches. The global notches being the notch geometries studied, and local notches being notches/defects caused by the poor surface quality distributed all over the

surface of the specimens, and the size of the defects being dependent on the amount of overhang.

5.1. Notch sensitivity

From the fatigue data obtained, the fatigue notch factor and notch sensitivity were evaluated and compared to the elastic stress concentration factor. According to the formulation of notch sensitivity [47], the notch sensitivity decreases, as the notch radius decreases. That is also the case for the AM Inconel 718 specimens investigated here; the notch sensitivity is decreased as the radius of the notch is decreased. The formulation of notch sensitivity states that if the notch has no effect, the notch sensitivity is equal to zero, while if the notch has a full effect, notch sensitivity is equal to one. For both v-notches, the notch sensitivity is between zero and one, as expected. The semi-circular notch, however, showed a notch sensitivity above one, which should not be possible.

The unnaturally high notch sensitivity obtained for semi-circular specimen can be explained by the specimens failing from lack of fusion defects, far away from the notch root, as seen in Fig. 12. The combination of notch sensitivity above one and specimens failing from defects in the downward facing region of the notch indicates that for this geometry the local defects are stronger mechanisms for fatigue than the global notch geometry. Further, it can be argued that the values obtained for notch sensitivity does not describe the material properties, but rather a combination of material and "component" properties, including geometrical effects from the build. Another possible factor influencing the unnaturally high notch sensitivity seen in the semi-circular specimens can be that the unnotched specimens have $K_t = 1.07$ and not $K_t = 1.00$. However, this should account for a small change in the value of notch sensitivity.

5.2. Scatter bands

In the case of the S-N data presented in Fig. 5, the size of the scatter bands for the different specimen geometries is decreasing as the notch radius is decreasing. The variation of defect size is decreasing as the notch radius is decreasing, so is the variation of the failure initiation site. These observations can be connected to the idea that fatigue is a weakest link mechanism. In the notched specimens the global notch is competing with the local defects, as blunt notch specimens show large defects and are not failing from the notch root, while when the notch radius is decreasing, the failure site is localising at the notch root again. For the unnotched specimens, it seems more arbitrary if there is a defect present and where it is located, as the surface region close to the gauge section has a low degree of overhang and the stress concentration is low and equal to $K_t = 1.07$.

5.3. Fractography

The fracture surfaces were investigated for all specimens, and it was found that all specimens had crack initiation from defects in the surface region. It was also found that unnotched specimens failed from one local defect, with no particular sign of lack of fusion, while the notched specimens failed from larger defects, caused by lack of fusion, distributed along the whole edge of the specimen.

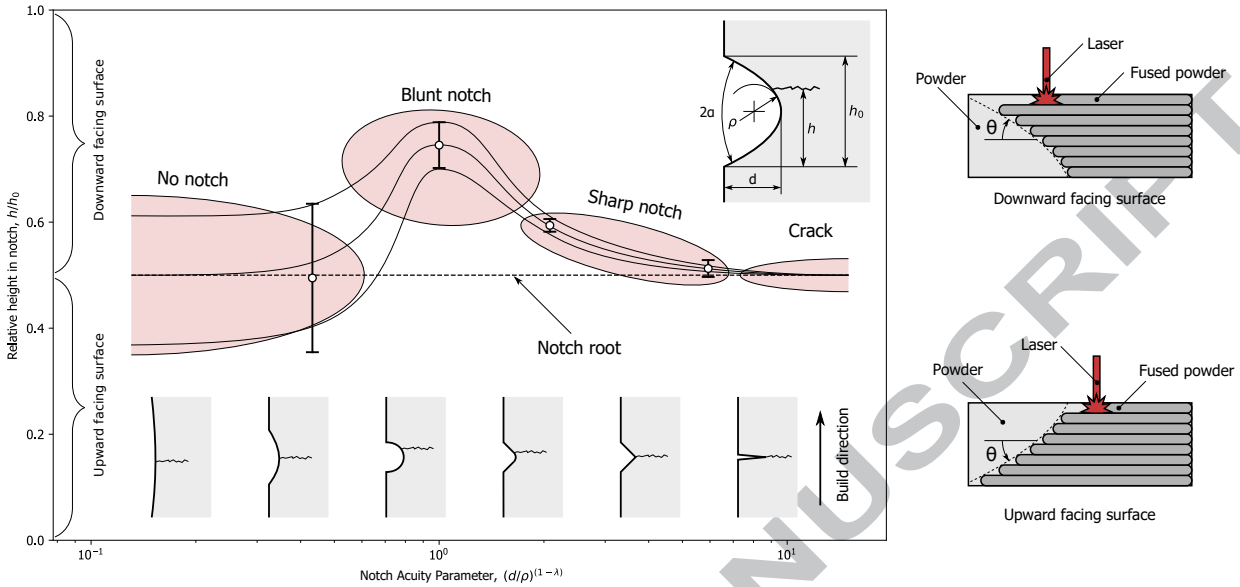

Figure 14: Diagram relating failure initiation site in a notched region to the notch acuity.

In this work the defect size is related to the fatigue life by the scatterbands, this is similar to the approach of Tammas-Williams et al. for machined Ti6Al4V specimens [13]. For the unnotched specimens, a strong dependence between the confidence band and the defect size was found, this was also seen in the specimens of Tammas-Williams et al. For the notch specimens less dependence between defect size and scatter bands was found, also the scatter bands were smaller.

5.4. Failure initiation site

The position of failure initiation site measured as relative height in notch, was obtained for all specimens. Results showed that the unnotched specimens had a large scatter in failure initiation sites, but on average the specimens failed from the centre. The semi-circular notch specimens have a weak stress concentration factor (K_t=1.31), and the failure was governed by the lack of fusion defects in the overhang region of the notch. With a decreasing notch radius and an increased stress concentration factor, the scatter was decreased, and the position of the failure site was moved closer to the notch root.

Based on these observations a diagram relating the position of failure to the acuity of the notch was created. The diagram is shown in Fig. 14, and is considering the average failure initiating position and standard deviation for each geometry, in terms of relative height in the notch, h/h_0. The acuity of the notch is described by a geometrical based parameter

$$\left(\frac{d}{\rho}\right)^{(1-\lambda)}, \tag{5}$$

where d is the depth of the notch, ρ is the notch radius and λ is the Williams' series eigenvalue [35], a parameter dependent on the notch opening angle. AM metal parts will always have a

finite resolution based on the accuracy of the manufacturing method, the notch radius will therefore never be zero, and the notch acuity parameter will always be defined. The dashed line in the diagram is representing the centre of the notch, e.i. the position of maximum stress.

The diagram shows that: (1) For a decreasing notch acuity, the scatter in failure initiation site is decreased. (2) At some combination of stress concentration due to the notch and amount of overhanging surface, the failure is occurring from the overhang region. (3) Gives some indication of whether the local defects or the notch geometry is controlling the failure initiation site. The diagram can easily be extended to other build orientations and altered based on the particularities of the AM method.

5.5. Strain Energy Density

When evaluating the structural integrity of AM metallic components it is evident that parameters such as residual stresses, geometrical defects, surface roughness, distortions and microstructure deriving from the manufacturing process are influencing factors. However, taking into account all of these parameters is a task too complex from a practical point of view. The process parameters used for additive materials are continuously being improved; hence, the aim of this work is not reporting the fatigue data from some specific process and material, but rather addressing a general problem related to the interaction between defects and component geometry, which to some degree will always be present in as-built AM components, e.g. machining of surfaces will not always be possible due to the geometrical complexity of the component. Energy based approaches such as ASED, not sensitive to mesh size, could be a way to deal with these kinds of problems; however, there are some challenges.

Few data exist of what should be used as the critical radius of Inconel 718. Notched fatigue data of Inconel 718 by Chen et al. [24], was analysed by use of critical distance by Louks and Susmel [46], using a critical distance of 0.15 mm. In the case of the AM specimens investigated here, a critical radius of 0.13 mm was used, which is close to the value proposed for critical distance. It should be noted that the material of Chen et al. was heat treated and machined, in contrast to the material considered here, which was produced by SLM and tested as-built. Also, the theory of critical distances and ASED are different, but the reported result of distance proposed by Louks and Susmel for critical distance can be taken as a reference value.

From the Atzori-Lazzarin diagram re-interpreted in terms of ASED it is evident that if either fracture mechanics or notch mechanics apply, ASED can be applied. However, in the case of the specimens investigated here, there is an interaction between local and global defects. Global defects can be considered by linear notch mechanics, and local defects can be considered by fracture mechanics, by for example the $\sqrt{\text{area}}$-method, as previously seen in literature for AM metals [13–17]. It should be noted that the $\sqrt{\text{area}}$-method only considers the defect area initiating fatigue and not the interaction of several defects.

Here, ASED of the specimens was evaluated to see if it was possible to present fatigue data for AM specimens in unified scatter bands, and to uncover challenges related to it.

The diagram proposed in Fig. 14 shows that based on a combination of notch acuity and amount of overhang, failure is controlled by local or global geometrical effects.

The results for ASED of the v-notch geometries in Fig. 13a, shows that both the v-notch geometries are coinciding with the unnotched fatigue strength at 2×10^6 cycles, with a scatter of $T_{\Delta W} = 1.45$. When also taking into account the value from the semi-circular notch, in Fig. 13b, the scatter is increased, and the data is not coinciding with the rest of the data. From the results, it seems that when the failure is initiating at notch tip or close to it, and the notch is a stronger and/or comparable strength as the local defects, it is possible to apply it. But in the case of the semi-circular specimens, the failure is governed by the local defects, and linear notch mechanics can not be applied. The threshold of which is the stronger factor for initiating fatigue, of the local and global defects, should be further studied in order develop understanding of which of them should be evaluated, and which could be taken as statistical scatter.

6. Conclusion

Fatigue assessment of different notched as-built AM Inconel 718 specimens produced by SLM has been conducted. The main findings can be summarised as:

1. Stress concentration factor, fatigue notch factor and notch sensitivity were obtained for the different geometries. The fatigue notch factor was increasing with deceasing notch radius. For the v-notched specimens, a notch sensitivity between zero and one was obtained, while for the semi-circular specimens, a notch sensitivity above one was obtained. This effect was assigned to the poor surface quality obtained building downward facing surfaces. It is also suggesting that the values obtained, when evaluating notch sensitivity of AM as-built specimens, are not valid as a material parameter, but rather as a material-component parameter.
2. The scatter in fatigue life and the scatter in the position of failure, with respect to the notch bisector line, in specimens was reduced with deceasing notch radius. This effect was assigned to the interaction between global and local stress risers, i.e. notch geometry and local defects from overhanging region. For low stress concentration from the notch geometry, the local defects are the stronger mechanism, and a large scatter is seen, while for stronger stress concentration from the notch geometry the failure is localising at the notch root.
3. All specimens were found to fail from defects in the surface region. The unnotched specimens failed from localised defects, while the notched specimens failed from larger defects, caused by lack of fusion, distributed along the whole edge of the notch. A strong dependency between the area of the defect and placement in confidence bands was found for unnotched specimens; a weaker dependency was obtained for notched specimens.
4. A diagram relating the scatter in failure position, with respect to the notch bisector line, to the notch acuity was proposed. The diagram gives an indication whether the notch geometry or the local defects is the driving mechanism for fatigue, and where failure can be expected in a notch geometry.

5. The fatigue data was analysed by means of ASED. The analysis showed that it was possible to present specimens failing from the notch root, or in the region close to it, in unified scatter bands.

Acknowledgement

Funding: This work was supported by the Norwegian Centre for International Cooperation in Education [PNA-2017/10077]; and Norwegian University of Science and Technology.

References

[1] J. Pegues, M. Roach, R. S. Williamson, N. Shamsaei, Surface roughness effects on the fatigue strength of additively manufactured ti-6al-4v, International Journal of Fatigue 116 (2018) 543 – 552. doi:https://doi.org/10.1016/j.ijfatigue.2018.07.013.
URL http://www.sciencedirect.com/science/article/pii/S0142112318302986

[2] J. J. Lewandowski, M. Seifi, Metal additive manufacturing: A review of mechanical properties, Annual Review of Materials Research 46 (1) (2016) 151–186. doi:10.1146/annurev-matsci-070115-032024.

[3] T. DebRoy, H. Wei, J. Zuback, T. Mukherjee, J. Elmer, J. Milewski, A. Beese, A. Wilson-Heid, A. De, W. Zhang, Additive manufacturing of metallic components process, structure and properties, Progress in Materials Science 92 (2018) 112 – 224. doi:https://doi.org/10.1016/j.pmatsci.2017.10.001.
URL http://www.sciencedirect.com/science/article/pii/S0079642517301172

[4] A. Yadollahi, N. Shamsaei, Additive manufacturing of fatigue resistant materials: Challenges and opportunities, International Journal of Fatigue 98 (2017) 14 – 31. doi:https://doi.org/10.1016/j.ijfatigue.2017.01.001.
URL http://www.sciencedirect.com/science/article/pii/S0142112317300014

[5] G. Nicoletto, Directional and notch effects on the fatigue behavior of as-built dmls ti6al4v, International Journal of Fatigue 106 (2018) 124 – 131. doi:https://doi.org/10.1016/j.ijfatigue.2017.10.004.
URL http://www.sciencedirect.com/science/article/pii/S0142112317303961

[6] R. Mertens, S. Clijsters, K. Kempen, J.-P. Kruth, Optimization of scan strategies in selective laser melting of aluminum parts with downfacing areas, Journal of Manufacturing Science and Engineering 136. doi:10.1115/1.4028620.

[7] D. Wang, Y. Yang, Z. Yi, X. Su, Research on the fabricating quality optimization of the overhanging surface in slm process, The International Journal of Advanced Manufacturing Technology 65 (9) (2013) 1471–1484. doi:10.1007/s00170-012-4271-4.
URL https://doi.org/10.1007/s00170-012-4271-4

[8] M. Seifi, A. Salem, J. Beuth, O. Harrysson, J. J. Lewandowski, Overview of materials qualification needs for metal additive manufacturing, JOM 68 (3) (2016) 747–764. doi:10.1007/s11837-015-1810-0.
URL https://doi.org/10.1007/s11837-015-1810-0

[9] R. Molaei, A. Fatemi, N. Phan, Significance of hot isostatic pressing (hip) on multiaxial deformation and fatigue behaviors of additive manufactured ti-6al-4v including build orientation and surface roughness effects, International Journal of Fatigue 7 (2018) 352 – 370. doi:https://doi.org/10.1016/j.ijfatigue.2018.07.035.
URL http://www.sciencedirect.com/science/article/pii/S0142112318303207

[10] S. Tammas-Williams, P. J. Withers, I. Todd, P. B. Prangnell, The effectiveness of hot isostatic pressing for closing porosity in titanium parts manufactured by selective electron beam melting, Metallurgical and Materials Transactions A 47 (5) (2016) 1939–1946. doi:10.1007/s11661-016-3429-3.

[11] S. Tammas-Williams, H. Zhao, F. Lonard, F. Derguti, I. Todd, P. Prangnell, Xct analysis of the influence of melt strategies on defect population in ti6al4v components manufactured by selective electron beam melting, Materials Characterization 102 (2015) 47 – 61.

427 doi:https://doi.org/10.1016/j.matchar.2015.02.008.
428 URL http://www.sciencedirect.com/science/article/pii/S104458031500039X
429 [12] S. M. J. Razavi, G. G. Bordonaro, P. Ferro, J. Torgersen, F. Berto, Fatigue behavior of porous ti-6al-4v
430 made by laser-engineered net shaping, Materials 11 (2). doi:10.3390/ma11020284.
431 URL http://www.mdpi.com/1996-1944/11/2/284
432 [13] S. Tammas-Williams, P. Withers, I. Todd, P. Prangnell, The influence of porosity on fatigue
433 crack initiation in additively manufactured titanium components, Scientific Reports 7 (2017) 7308.
434 doi:https://doi.org/10.1038/s41598-017-06504-5DO.
435 [14] H. Masuo, Y. Tanaka, S. Morokoshi, H. Yagura, T. Uchida, Y. Yamamoto, Y. Murakami,
436 Influence of defects, surface roughness and hip on the fatigue strength of ti-6al-4v manu-
437 factured by additive manufacturing, International Journal of Fatigue 117 (2018) 163 – 179.
438 doi:https://doi.org/10.1016/j.ijfatigue.2018.07.020.
439 [15] G. Meneghetti, D. Rigon, C. Gennari, An analysis of defects influence on axial fatigue strength of
440 maraging steel specimens produced by additive manufacturing, International Journal of Fatigue 118
441 (2019) 54 – 64. doi:https://doi.org/10.1016/j.ijfatigue.2018.08.034.
442 [16] J. Gunther, D. Krewerth, T. Lippmann, S. Leuders, T. Troster, A. Weidner, H. Biermann, T. Niendorf,
443 Fatigue life of additively manufactured ti6al4v in the very high cycle fatigue regime, International
444 Journal of Fatigue 94 (2017) 236 – 245, fatigue and Fracture Behavior of Additive Manufactured Parts.
445 doi:https://doi.org/10.1016/j.ijfatigue.2016.05.018.
446 [17] Y. Yamashita, T. Murakami, R. Mihara, M. Okada, Y. Murakami, Defect analysis and fatigue design
447 basis for ni-based superalloy 718 manufactured by selective laser melting, International Journal of
448 Fatigue 117 (2018) 485 – 495. doi:https://doi.org/10.1016/j.ijfatigue.2018.08.002.
449 [18] Y. Murakami, Chapter 2 - stress concentration, in: Y. Murakami (Ed.), Metal Fatigue, Elsevier Science
450 Ltd, Oxford, 2002, pp. 11 – 24. doi:https://doi.org/10.1016/B978-008044064-4/50002-5.
451 URL http://www.sciencedirect.com/science/article/pii/B9780080440644500025
452 [19] F. Berto, P. Lazzarin, Recent developments in brittle and quasi-brittle failure assessment of engineering
453 materials by means of local approaches, Materials Science and Engineering: R: Reports 75 (2014) 1 –
454 48. doi:https://doi.org/10.1016/j.mser.2013.11.001.
455 [20] G. Meneghetti, A. Campagnolo, F. Berto, B. Atzori, Averaged strain energy density evaluated rapidly
456 from the singular peak stresses by fem: cracked components under mixed-mode (i+ii) loading, The-
457 oretical and Applied Fracture Mechanics 79 (2015) 113 – 124, recent development of Energy density
458 methods: Mechanics of solids (EDMS). doi:https://doi.org/10.1016/j.tafmec.2015.08.001.
459 URL http://www.sciencedirect.com/science/article/pii/S0167844215300847
460 [21] A. Campagnolo, G. Meneghetti, F. Berto, Rapid finite element evaluation of the av-
461 eraged strain energy density of mixed-mode (i+ii) crack tip fields including the t-stress
462 contribution, Fatigue & Fracture of Engineering Materials & Structures 39 (8) 982–998.
463 arXiv:https://onlinelibrary.wiley.com/doi/pdf/10.1111/ffe.12439, doi:10.1111/ffe.12439.
464 URL https://onlinelibrary.wiley.com/doi/abs/10.1111/ffe.12439
465 [22] G. Meneghetti, A. Campagnolo, F. Berto, Averaged strain energy density estimated
466 rapidly from the singular peak stresses by fem: Cracked bars under mixed-mode (i+iii)
467 loading, Engineering Fracture Mechanics 167 (2016) 20 – 33, sI:CRACK PATHS 2015.
468 doi:https://doi.org/10.1016/j.engfracmech.2016.03.040.
469 URL http://www.sciencedirect.com/science/article/pii/S0013794416301461
470 [23] S. Razavi, P. Ferro, F. Berto, J. Torgersen, Fatigue strength of blunt v-notched specimens produced by
471 selective laser melting of ti-6al-4v, Theoretical and Applied Fracture Mechanics 97 (2018) 376 – 384.
472 doi:https://doi.org/10.1016/j.tafmec.2017.06.021.
473 [24] Q. Chen, N. Kawagoishi, H. Nisitani, Evaluation of notched fatigue strength at elevated tem-
474 perature by linear notch mechanics, International Journal of Fatigue 21 (9) (1999) 925 – 931.
475 doi:https://doi.org/10.1016/S0142-1123(99)00081-X.
476 URL http://www.sciencedirect.com/science/article/pii/S014211239900081X
477 [25] N. Kawagoishi, Q. Chen, H. Nisitani, Fatigue strength of inconel 718 at elevated tem-

peratures, Fatigue & Fracture of Engineering Materials & Structures 23 (3) 209–216. arXiv:https://onlinelibrary.wiley.com/doi/pdf/10.1046/j.1460-2695.2000.00263.x, doi:10.1046/j.1460-2695.2000.00263.x.
URL https://onlinelibrary.wiley.com/doi/abs/10.1046/j.1460-2695.2000.00263.x

[26] D. Witkin, D. Patel, G. Bean, Notched fatigue testing of inconel 718 prepared by selective laser melting, Fatigue & Fracture of Engineering Materials & Structures 0 (0). arXiv:https://onlinelibrary.wiley.com/doi/pdf/10.1111/ffe.12880, doi:10.1111/ffe.12880.
URL https://onlinelibrary.wiley.com/doi/abs/10.1111/ffe.12880

[27] R. Konen, L. Kunz, G. Nicoletto, A. Baa, Long fatigue crack growth in inconel 718 produced by selective laser melting, International Journal of Fatigue 92 (2016) 499 – 506, fatigue crack paths 2015. doi:https://doi.org/10.1016/j.ijfatigue.2016.03.012.
URL http://www.sciencedirect.com/science/article/pii/S0142112316300172

[28] H. Neuber, Kerbspannungslehre, Springer-Verlag, 1958.

[29] H. Neuber, ber die bercksichtigung der spannungskonzentration bei festigkeitsberechnungen, Konstruktion 20 (7) (1968) 245–251, cited By 246.

[30] E. Beltrami, Sulle condizioni di resistenza dei corpi elastici, rend. r. ist. lombardo di scienze, Lettere e Arti 18 (1885) 704, cited By 1.

[31] G. Sih, B. Cha, A fracture criterion for three-dimensional crack problems, Engineering Fracture Mechanics 6 (4) (1974) 699 – 723. doi:https://doi.org/10.1016/0013-7944(74)90068-X.
URL http://www.sciencedirect.com/science/article/pii/001379447490068X

[32] Mechanics of Fracture Initiation and Propagation, Kluwer, 1991.

[33] P. Lazzarin, R. Zambardi, A finite-volume-energy based approach to predict the static and fatigue behavior of components with sharp v-shaped notches, International Journal of Fracture 112 (3) (2001) 275–298. doi:10.1023/A:1013595930617.
URL https://doi.org/10.1023/A:1013595930617

[34] P. Lazzarin, R. Tovo, A unified approach to the evaluation of linear elastic stress fields in the neighborhood of cracks and notches, International Journal of Fracture 78 (1996) 3–19.

[35] M. L. Williams, On the stress distribution at the base of a stationary crack, Journal of Applied Mechanics 24(1) (1956) 109–114.

[36] F. Berto, A. Campagnolo, P. Lazzarin, Fatigue strength of severely notched specimens made of ti6al4v under multiaxial loading, Fatigue & Fracture of Engineering Materials & Structures 38 (5) (2014) 503–517. arXiv:https://onlinelibrary.wiley.com/doi/pdf/10.1111/ffe.12272, doi:10.1111/ffe.12272.
URL https://onlinelibrary.wiley.com/doi/abs/10.1111/ffe.12272

[37] G. Meneghetti, A. Campagnolo, F. Berto, K. Tanaka, Notched ti-6al-4v titanium bars under multiaxial fatigue: Synthesis of crack initiation life based on the averaged strain energy density, Theoretical and Applied Fracture Mechanics 96 (2018) 509 – 533. doi:https://doi.org/10.1016/j.tafmec.2018.06.010.
URL http://www.sciencedirect.com/science/article/pii/S0167844218300983

[38] A. Campagnolo, G. Meneghetti, F. Berto, K. Tanaka, Crack initiation life in notched steel bars under torsional fatigue: Synthesis based on the averaged strain energy density approach, International Journal of Fatigue 100 (2017) 563 – 574, multiaxial Fatigue 2016: Experiments and Modeling. doi:https://doi.org/10.1016/j.ijfatigue.2016.12.022.
URL http://www.sciencedirect.com/science/article/pii/S0142112316304297

[39] B. Atzori, P. Lazzarin, Notch sensitivity and defect sensitivity under fatigue loading: Two sides of the same medal, International Journal of Fracture 107 (1) (2001) 1–8. doi:10.1023/A:1007686727207.
URL https://doi.org/10.1023/A:1007686727207

[40] P. Lazzarin, F. Berto, From neuber's elementary volume to kitagawa and atzori's diagrams: An interpretation based on local energy, International Journal of Fracture 135 (1) (2005) L33–L38. doi:10.1007/s10704-005-4393-x.
URL https://doi.org/10.1007/s10704-005-4393-x

[41] H. Kitagawa, S. Takahashi, Applicability of fracture mechanics to very small cracks in the early stage, in: Procs. Second International Conference on Mechanical Behaviour of Materials.

[42] W. D. Pilkey, D. F. Pilkey, Peterson's Stress Concentration Factors, Wiley, New Yersey, 2008.
[43] ASTM E407-07(2015)e1, Standard Practice for Microetching Metals and Alloys, ASTM International, West Conshohocken, PA, 2015, www.astm.org.
[44] Inconel alloy 718, Tech. rep., Special Metals (2018).
[45] R. Branco, J. D. M. Costa, F. Berto, S. M. J. Razavi, J. A. M. Ferreira, C. Capela, L. Santos, F. Antunes, Low-cycle fatigue behaviour of aisi 18ni300 maraging steel produced by selective laser melting, Metals 8 (1). doi:10.3390/met8010032.
URL http://www.mdpi.com/2075-4701/8/1/32
[46] R. Louks, L. Susmel, The linear-elastic theory of critical distances to estimate high-cycle fatigue strength of notched metallic materials at elevated temperatures, Fatigue & Fracture of Engineering Materials & Structures 38 (6) (2014) 629–640. arXiv:https://onlinelibrary.wiley.com/doi/pdf/10.1111/ffe.12273, doi:10.1111/ffe.12273.
URL https://onlinelibrary.wiley.com/doi/abs/10.1111/ffe.12273
[47] H. Neuber, Theory of Notch Stresses, 2nd Edition, Springer, Berlin, 1958.

Nomenclature

AM	Additive Manufacturing
ASED	Average Strain Energy Density
CT	Computed Tomography
FE	Finite Element
HIP	Hot Isostatic Pressing
PBF	Powder Bed Fusion
SED	Strain Energy Density
SEM	Scanning Electron Microscopy
SLM	Selective Laser Melting
2α	Notch opening angle
a, d	Crack/Notch depth
a_0	Lower threshold value of notch depth
a^*	Short crack/notch
A_d	Total defect area
ΔK_I	Notch Stress Intensity Range
$\Delta\sigma$	Stress range
$\Delta\sigma^S$	Stress range unnotched specimen
$\Delta\sigma^N$	Stress range notched specimen
E	Young's Modulus
h	Failure site in notch
h_0	Height of notch opening in build direction
K_I^V	Generalised stress intensity factor
k	Inverse slope of scatter bands
K_f	Fatigue notch factor
K_t	Stress concentration factor
λ_I	Eigenvalue of Willams' series
N_f	Number of cycles to failure
q	Notch sensitivity
R	Loading ratio
R_0	Critical radius
r_0	Centroid of critical radius
ρ	Notch radius
σ_t	Tensile strength
σ_{max}	Maximum stress
$T_{\Delta\sigma}$	Scatter parameter
$\bar{W}$	Average Strain Energy Density
W_c	Critical Average Strain Energy Density

Graphical Abstract

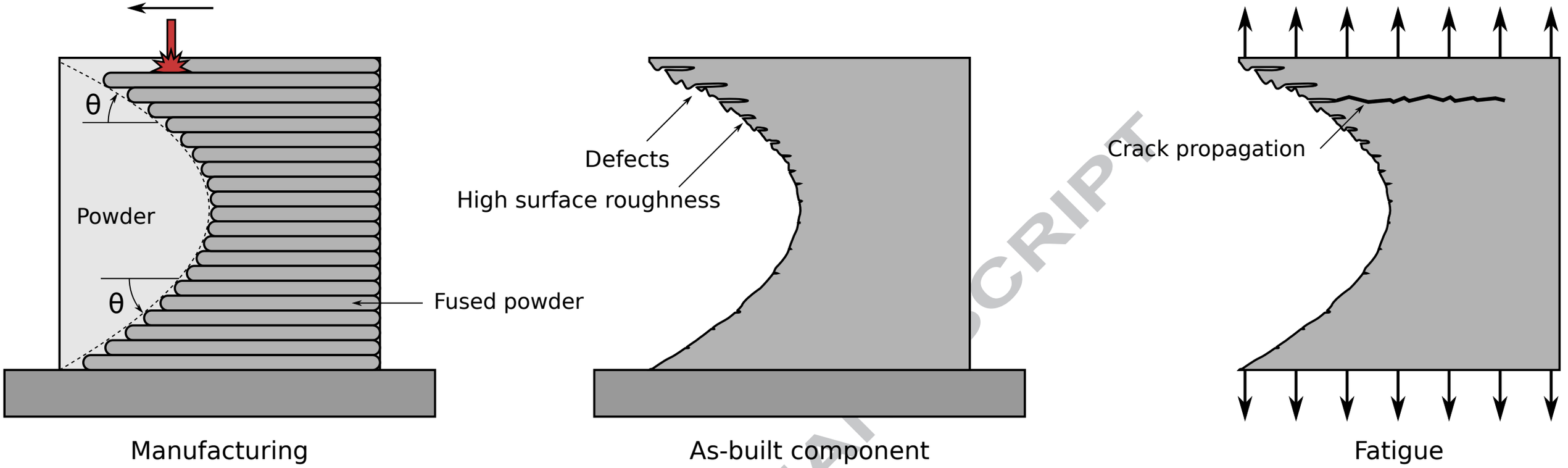

Notch-Defect Interaction in Additively Manufactured Inconel 718

K. Solberg, F. Berto

Department of Mechanical and Industrial Engineering, Norwegian University of Science and Technology, 7034 Trondheim, Norway

Highlights

- Specimens fail from defects in surfaces build facing downwards
- Size of measurable defects in fracture surface is related to the fatigue life
- A diagram relating the position of failure initiation site to the notch acuity is proposed
- Average strain energy density failure criteria is able to predict fatigue life for sharp notches